$K^h\alpha_{1,2}$ hypersatellites of 3*d* transition metals and their photoexcitation energy dependence

R. Diamant,[1] S. Huotari,[2] K. Hämäläinen,[3,*] R. Sharon,[1] C. C. Kao,[4] and M. Deutsch[1]
[1]*Department of Physics, Bar-Ilan University, Ramat-Gan 52900, Israel*
[2]*ESRF, 6 rue Jules Horowitz, BP 220, F-38043 Grenoble Cedex, France*
[3]*Department of Physics, University of Helsinki, P.O. Box 64, FI-00014 Helsinki, Finland*
[4]*NSLS, Brookhaven National Laboratory, Upton, New York 11973, USA*
(Received 15 December 2008; revised manuscript received 16 March 2009; published 25 June 2009)

Hollow atoms in which the *K* shell is empty while the outer shells are populated allow studying a variety of important and unusual properties of atoms. The diagram x-ray emission lines of such atoms, the $K^h\alpha_{1,2}$ hypersatellites (HSs), were measured for the 3*d* transition metals, $Z=23-30$, with a high energy resolution using photoexcitation by monochromatized synchrotron radiation. Good agreement with *ab initio* relativistic multiconfigurational Dirac-Fock calculations was found. The measured HS intensity variation with the excitation energy yields accurate values for the excitation thresholds, excludes contributions from shake-up processes, and indicates domination near threshold of a nonshake process. The *Z* variation of the HS shifts from the diagram line $K\alpha_{1,2}$, the $K^h\alpha_1-K^h\alpha_2$ splitting, and the $K^h\alpha_1/K^h\alpha_2$ intensity ratio, derived from the measurements, are also discussed with a particular emphasis on the QED corrections and Breit interaction.

DOI: 10.1103/PhysRevA.79.062511 PACS number(s): 32.30.Rj, 32.70.−n, 32.80.Fb

I. INTRODUCTION

Satellite lines in x-ray spectra were recognized as early as 1916 to originate from multielectronic transitions within an atom [1]. They should reflect, therefore, any electron-electron interactions existing within the atom [2,3]. Such interactions go beyond the independent electron model of the atom, where each electron is considered to interact with the nucleus only, independent of the other electrons. They also go beyond the frozen-core–sudden-approximation picture of electronic excitations, where the initial hole states are formed by a sudden ejection of an electron, keeping the atomic shell structure frozen in the ground state configuration [2,4]. This picture is particularly inappropriate for excitations near threshold, where the ejected low-velocity electrons stay within the bounds of the atom over a time scale comparable with that required for shell relaxation due to the holes created. Here the excitation process and the de-excitation by an x-ray photon or an Auger electron emission can no longer be considered as independent processes. In this regime, denoted as the adiabatic limit [5], the excitation and de-excitation processes merge into a single process, rather than the two consecutive ones occurring in the isothermal sudden-approximation limit, where infinitely fast electron ejection occurs, and the de-excitation occurs before significant shell relaxation can take place.

The particular multielectronic spectra studied here, the *K*-shell hypersatellites (HSs), denoted $K^h\alpha_{1,2}$, originate in $[1s]^{-2}(^1S_0)\rightarrow[1s2p]^{-1}(^{1,3}P_1)$ transitions ($[nl]^{-x}$ denote *x* vacancies in the *nl* shell). They are of particular interest for several reasons. Involving two vacancies in the same shell in their initial state, they allow studying *intrashell* interactions. The influence of relativity on electron interactions should also be reflected in the spectra as the *K* shell is strongly relativistic in the *Z* range addressed here. In addition, the $K^h\alpha_1$ line originates in a transition requiring a spin flip, which is dipole forbidden in the pure *LS* coupling scheme and is fully allowed only in the *jj* scheme [6,7]. Thus, the intensity ratio $R=I(K^h\alpha_1)/I(K^h\alpha_2)$ provides the most sensitive (and almost only) way to measure the variation in the coupling of atomic angular momenta across the Periodic Table with an increasing *Z* from the *LS*, through the intermediate, to the *jj* coupling scheme [8]. The $K^h\alpha_{1,2}$ HS spectra are also unique in allowing to study the Breit interaction, the most elusive and least studied of all atomic interactions. The Coulomb interaction dominates almost all atomic transitions, with the Breit contribution being $<1\%$. However, for the shift of the HS lines from their corresponding diagram lines a partial cancelation of the Coulomb contribution occurs, rendering the Breit contribution as high as 20% at high *Z* [9,10,4]. Quantum electrodynamic (QED) effects can also be accessed experimentally in the HS spectra through their significant contribution to the splitting of the two lines in the $K^h\alpha_{1,2}$ spectrum [10,11].

The HS spectrum is also the "diagram" spectrum of a *hollow atom* [12]. This term, introduced by Briand *et al.* [13], denotes an atom with an empty inner shell while its outer shells are populated as in a neutral unexcited atom. The formation, properties, and decay modes of such atoms are of profound interest to fundamental atomic physics [12–17]. They provide an insight into the behavior of atoms very far from equilibrium and into ultrafast dynamics in atoms [18]. They have a wide range of applications, actual and potential, in physics, chemistry, biology, and materials science, particularly in the study of the near-surface electronic structure of solids [12,19,20]. Hollow atoms are also being studied as a way to achieve population inversion and lasing in the hard x-ray regime [20,21]. For all these reasons, hollow atoms are an active field of theoretical and experimental research [12,18,22]. For all but the lowest-*Z* atoms (He, H, and Li) hollow atoms were almost exclusively created to date by electron pickup from metallic [13] or insulating [23] surfaces by highly charged stripped ions traveling close to the surface.

*keijo.hamalainen@helsinki.fi

This process does not allow an accurate control of the charge state and of the specific shell filling of the hollow atom. Studies of hollow atoms prepared by the much better controlled single-photon [15] or multiphoton [20,24] excitation processes [25] are scarce, particularly for levels requiring hard x rays [11,26–28].

HSs were first detected experimentally by Briand *et al.* [29], employing nuclear K electron capture in a radioactive atom. In electron capture, the initial state holes are created over a virtually zero time scale, and the process is well approximated by the sudden-approximation frozen-core model of photoionization [30]. This excitation mode suffers, however, from being restricted to those elements exhibiting electron capture. Moreover, the low activity of the available radioactive materials yields a very low intensity for the resulting HS spectra. The Z^{-2} decrease of the K capture probability [31] further reduces the intensity as Z is increased. Thus, studies employing nuclear decay processes lack the intensity to allow high-resolution measurements of the HS spectra. In contrast, heavy ion collisions provide a 100-fold increase in the HS excitation cross section as compared to nuclear decay processes [32]. This, however, is achieved at a cost: heavy ion collisions are violent events, producing a plethora of higher-order multivacancy states. The resulting spectra contain a highly overlapping composite of higher-order spectra, and separating out the HS spectrum is neither easy nor accurate [33]. Moreover, it has been demonstrated that the intensity of the HS spectra in heavy ion collisions increases in quadrature with the intensity of the impinging ion beam. This indicates that the two K vacancies are generated in two independent single ionization events [33,34] rather than by an electron-electron interaction mediated electron ejection following a single ionization event. Thus, initial state correlation effects are only marginally reflected in HS spectra generated in heavy atom collisions. Light ion [33,35] and electron [34,36] excitations were also employed in HS studies, the former suffering from a low intensity and the latter from a high background due to bremsstrahlung.

HS excitation by photons has several advantages over the methods discussed above. The single-particle nature of the photon-electron interaction allows only one electron to be ionized directly by the incoming photon. The ejection of a second electron and thus the formation of the initial $[1s]^{-2}$ state of a HS line can only occur because of electron-electron interactions [3]. In addition, the probability of photoexciting more than two electrons is negligible, resulting in pure HS spectra, uncontaminated by higher-order lines and free from bremsstrahlung-generated background. However, the low intrinsic cross section of creating the $[1s]^{-2}$ hole state, on order of 10^{-4} of that of the diagram spectra in our Z range, requires a very high photon flux in order to obtain reasonable count rates for the emitted HS spectra. Such fluxes became available over the last decade, with the advent of synchrotron beamlines (mostly third generation) equipped with insertion devices, low band pass monochromators, and high-resolution, high-efficiency crystal spectrometers [11,37,38]. The insertion devices' high flux and the synchrotron's intrinsic time structure also allowed developing sophisticated coincidence methods for the weak HS spectra of medium-Z atoms such as Mo and Ag [15–17]. Other important developments over the last decades, relevant to this study, are the increase in computing power and the development of ever-more sophisticated atomic structure codes [39,40], which allow a detailed comparison of the well-resolved spectra measured at such beamlines with *ab initio* calculations. This should enable one, in principle, to extract the specific interactions, processes, and effects contributing to specific spectral features and determine their relative importance. The current status of the theoretical research in this field is summarized briefly in two recent theoretical [41,42] and two recent experimental [16,17] papers.

An extremely important property of photoexcitation by monochromatic synchrotron radiation is the possibility to vary the energy of the exciting photons. This allows one to explore the evolution of the various spectral features (line shape, peak positions, excitation cross sections, etc.) with excitation energy from the energy threshold for creating the initial state, through the near-threshold adiabatic regime toward the high-excitation-energy isothermal regime, where the intensity and other spectral features saturate. Such excitation-energy-dependent measurements, carried out for spectra arising from initial $[1s3d]^{-1}$ [43], $[1s2p]^{-1}$ [44–46], and $[1s]^{-2}$ [11] states in copper, revealed the strong dependence of the saturation range, edge behavior, and underlying ejection process on the shell and subshell, n and l, of the correlation-ejected electron. These studies also revealed a deviation, which increased as n and l decreased, of the perturbation-theoretical predictions of shake theory [47] from the measurements. Unfortunately, copper is the only atom for which such measurements of both excitation energy and n and l dependence were published to date. A full understanding and atomic structure modeling of this behavior will have to await the availability of such measurements for a significant range of atomic numbers Z.

A step in this direction is presented here as a high-resolution experimental study of the HSs, and their evolution from threshold with increasing excitation energy, for the $3d$ transition elements, $Z=23-30$. This Z range is of particular interest since the coupling varies here rapidly with Z from an almost pure LS coupling at the low end, vanadium, to the pronouncedly intermediate coupling at the high end, zinc [48]. We stress that the various processes and effects underlying the HS spectra are reflected in the energy positions, line splittings, and intensity ratio of the individual lines comprising the spectra. To properly address the relevant issues it is therefore imperative to have fully resolved HS spectra with a good statistical accuracy. For most of the spectra studied here no such previous data or only partial previous data are available in the literature. Moreover, no single systematic resolved study is available for the full Z range. The closest is that of Ahopelto *et al.* [49] for $Z=24$, 26, and 28, with error bars on the order of ~ 2 eV, 10-fold larger than in the present study. The evolution of the full spectra with excitation energy was published only for Cu by Diamant *et al.* [11] and for V by Huotari *et al.* [26] and by Oura *et al.* [28].

We have recently shown that the near-threshold evolution of the intensity of all measured HSs in our Z range follows a universal scaling behavior [50]. The universal evolution curve was shown to deviate from that predicted by shake theory [47] but agreed well with the curve calculated assum-

TABLE I. Experimental setup for each of the samples. Anl, Res, and Cal are the analyzer, the analyzer's resolution, and the calibration line, respectively. $[1s]^{-2}$ and $K^h\alpha_2$ energies were calculated with the $Z+1$ approximation [7]. Calibration energies are taken from Bearden [56]. Numbers in parentheses are the uncertainties in the last digits of the numbers cited.

Sample	Anl	$E(K^h\alpha_2)$ (keV)	Res (eV)	$E([1s]^{-2})$ (keV)	Cal	E_{cal} (keV)
V	Si(331)	5.1801	1.7	11.228	V $K\beta_{1,3}$	5.42729(5)
Cr	Si(422)	5.6512	0.9	12.292	Sm $L\alpha_1$	5.6361(5)
Mn	Si(333)	6.1445	1.7	13.405	Re $L\beta_2$	10.2752(3)[a]
Fe	Si(440)	6.6587	1.8	14.5643	Ho $L\alpha_2$	6.6795(7)
Co	Ge(620)	7.1926	2.4	15.773	Tm $L\alpha_1$	7.1799(8)
Ni	Ge(444)	7.7501	1.6	17.034	Au $L\alpha_1$	9.7133(2)[b]
Cu	Si(444)	8.3238	2.8	18.345	W $L\alpha_2$	8.3352(1)
Zn	Si(355)	8.9201	1.3	19.721	Cu $K\beta$	8.90529(6)

[a]Measured with the Si(555) reflection.
[b]Measured with the Ge(555) reflection.

ing the double K-shell ionization to be a semiclassical knock-out (KO) process [14,51,52] whereby the directly ionized K electron knocks out, billiardlike, the second K electron on its way out. However, our study (Ref. [50]) focused on the near-threshold evolution of the HS intensity only and did not provide information on the shape of the HS spectrum, the quantities of physical interest derived therefrom ($K^h\alpha_1-K^h\alpha_2$ line splittings, linewidths, intensity ratio R, $K^h\alpha_2-K\alpha_2$ shifts, etc.) and their variation with Z. These results, and more, are presented and discussed here along with fits of the measured spectra by theoretical spectra calculated *ab initio* using a relativistic multiconfigurational Dirac-Fock (RMCDF) method.

In the following we first discuss the methods of measurement and data analysis used in this study, followed by a presentation of the HS spectra and their energy and Z dependences as measured for the $3d$ transition elements, $Z=23-30$. A companion paper [53] will discuss our results for the $4d$ transition elements, obtained using a different experimental setup, dictated by the high-excitation energies and low cross sections involved.

II. EXPERIMENT

A. Beamline and spectrometer setup

Measurements were carried out at beamline X25, NSLS, Brookhaven National Laboratory, USA, and beamline ID16, ESRF, France. The setup at the NSLS included radiation from a wiggler, which was focused by a toroidal mirror and monochromatized by a two-bounce Si(111) monochromator. The resulting incident beam had at 20 keV an ~ 6 eV band pass and flux of $\sim 5\times 10^{11}$ photons/s, within a focus of ~ 0.5 mm^2. The incident excitation energy was tunable within the range of 6 keV$\leq E_{ex}\leq$25 keV. The incident beam's intensity was monitored by an ion chamber upstream of the sample. The radiation at ID16 was generated by two consecutive undulators, monochromatized by a Si(111) double-crystal monochromator, and focused at the sample by a toroidal mirror. The band pass at 19 keV was ~ 5 eV, with a flux of $\sim 10^{13}$ photons/s within a focus of 50×130 μm^2 ($V\times H$). The incident-beam intensity was monitored with a Si pin diode observing scattering from a Kapton foil downstream from the toroidal mirror.

The samples were high-purity (99.9% for V, Fe, Co, Ni, Cu, and Zn and unspecified high purity for Cr and Mn) metal plates or foils of a known thickness, so that the absorption of the incident and emitted radiations within the sample could be corrected for.

Prior to the measurements, a simple calculation was carried out to determine the threshold energy for exciting the initial state, $E([1s]^{-2})$, of each spectrum using the $Z+1$ approximation [7] with known binding energies [54]. The incident beam's energy was then calibrated to $\lesssim 2$ eV by measuring an absorption edge of an element having an edge of a known energy [54–56] in this region using the monitor ion chamber as a detector. The predicted position of the $K^h\alpha_2$ emission line, necessary for choosing the analyzer crystal, was also calculated using the $Z+1$ approximation [7]. The corresponding values are listed in Table I.

The $K^h\alpha_{1,2}$ emission spectra were recorded using a Johann-type spectrometer, with a Rowland circle of a diameter of 1 m on a horizontal plane. The analyzers were spherically bent Si or Ge crystals with diameters between 50 and 100 mm. The surface-parallel reflecting (hkl) planes of the analyzers were chosen for each sample to provide a Bragg angle θ_B as close to 90° as possible. Since most contributions to the energy resolution of the spectrometer are proportional to cot θ_B, this ensured as high a resolution as possible [37]. The analyzer crystals and planes employed for each sample are listed in Table I. The angles of the incident and detected beams were both kept at 45° relative to the sample's surface. Due to the natural linear polarization of the synchrotron radiation, the resulting 90° scattering angle minimized the amount of elastic and inelastic scattering and thus the background. The radiation reflected by the analyzer crystal was detected by a liquid nitrogen-cooled intrinsic Ge solid state detector with an energy resolution of $\lesssim$250 eV at the relevant energies. This, in conjunction with a fast amplifier and a single channel analyzer, ensured a very low background,

$\lesssim$0.01 counts/s, necessary for measuring these low-intensity spectra.

The spectrometer's energy scale was calibrated in each case by measuring a strong emission line of a known energy [54–56] from a separate calibration sample. The calibration sample's intensity was also used to calculate the intensity of the hypersatellite as a function of E_{ex}, relative to the diagram $K\alpha_{1,2}$ spectrum of the same element.

Two basic types of scans were carried out. In the first, the monochromator, and thus E_{ex}, was scanned, keeping the analyzer energy fixed at, e.g., the peak of the $K^h\alpha_2$ line. This yielded the threshold energy for exciting the spectrum as well as the peak intensity evolution with increasing E_{ex}. When the shape of the HS spectrum does not change with E_{ex}, as is the case here, a simple multiplication converts this curve from the evolution of the peak intensity to the evolution of the total intensity of the HS spectrum. Moreover, when the total intensity evolution curve is divided by the intensity variation curve of the $K\alpha$ diagram line over the same E_{ex} range [either measured directly or scaled from a measurement of another diagram line (see, e.g., Ref. [11])], the widely used partial fluorescence yield (PFY) curve $I(K^h\alpha)/I(K\alpha)$ of the HS spectrum is obtained.

In the second type of scan, the analyzer, and thus the emission energy E_{em}, was scanned, keeping E_{ex} fixed. This yields an emission spectrum at a fixed excitation energy. Several additional scans were also carried out, such as E_{ex} scans away from the spectrum's peaks' positions and E_{em} scans below excitation threshold. These were used to remove the backgrounds for the intensity evolution curves and emission spectra, respectively. Rather than using a single scan, with a long counting time at each point, we employed repeated scans, with short counting time at each point, which were summed up. This method minimized the influence of possible instabilities (none was found) and ensured the consistency of the data.

B. Data analysis

1. Data corrections

All spectra were corrected for the synchrotron's incident-beam intensity variation as measured by the monitor, the absorption in the sample of both incident and emitted radiations, and the dead time of the detector and its associated electronics, as described in detail in Ref. [11]. Off-peak and below-threshold background scans, corrected in the same way, were subtracted off the corrected spectra. The data sets obtained after this subtraction were considered to be clean, background-free, HS spectra which served for further analysis as described below. The statistical counting uncertainties of the points in the various scans that were used to calculate the final HS spectra (monitor and detector counts for both signal and background) were employed to calculate the error bars of each data point in the final HS spectra and in the evolution (PFY) curves according to standard error propagation formulas. The uncertainties listed for the peak energies of the HS spectra reflect the uncertainties in the energies of the diagram lines used to calibrate the emission energy scale, as well as the additional uncertainty due to the interpolation of the energy scale between these values. The uncertainties in quantities derived from fits of analytic forms to the data include fit uncertainties calculated by the least-squares fitting code used.

2. Phenomenological fit

To obtain an analytic description of the spectra, which is useful for calculating several of the quantities addressed by previous authors and for separating HS spectra from overlapping spectra containing higher-order transitions, a phenomenological fit of the spectrum by a minimal number of Voigt functions (VFs) was carried out. The VF is a convolution of a Gaussian, representing the instrumental resolution function, and a Lorentzian, representing the intrinsic emission line shape. A common Gaussian width was employed for all lines in the spectrum while the width, height, and position of each Lorentzian component were allowed to vary. In all cases, a single VF per spectral line (e.g., $K^h\alpha_2$) was sufficient to describe the measured line adequately.

3. Ab initio calculations

Each of the emission spectra measured in this study was also calculated *ab initio*, using the RMCDF code GRASP [40] in the average-level (AL) optimization mode, with supplementary code written in house. The fully J-split relativistic configurations were generated automatically in each run by GRASP from the input list of the electronic occupation numbers of the (nonrelativistic) shells. The wave functions and level energies were then calculated in the AL optimization mode. Two separate runs were carried out, one for the initial, $[1s]^{-2}$, and one for the final, $[1s2p]^{-1}$, states of the transitions producing the $K^h\alpha_{1,2}$ HS spectrum. The transition *energies* among the levels were then obtained by subtracting the appropriate level energies of the initial and final states, taking into consideration, of course, the selection rules of dipole-allowed transitions. As the wave functions of the initial and final states were generated in separate runs from different configurations they are not orthogonal and cannot be used in conjunction to calculate the intensities of the transitions. Hence, the relative *intensity* of each transition line was obtained in a configuration interaction calculation, using, in separate runs, the initial state wave functions and the final state wave functions. As was the case in previous calculations of this sort [11,44,45,57], the intensities obtained from these two calculations were very close to each other for all lines having intensities $>5-10$ % of the strongest line of the multiplet. These energy and intensity values were employed to construct the conventional "stick diagram," shown, for example, in Fig. 1. Further details of the calculations can be found in Refs. [11,44,45,57].

The stick diagram allowed us to calculate the theoretical energy position for each peak, as a weighted average over the relevant group of sticks, the splitting $\delta=E(K^h\alpha_2)-E(K^h\alpha_1)$ of the two lines in the $K^h\alpha_{1,2}$ multiplet, the shift

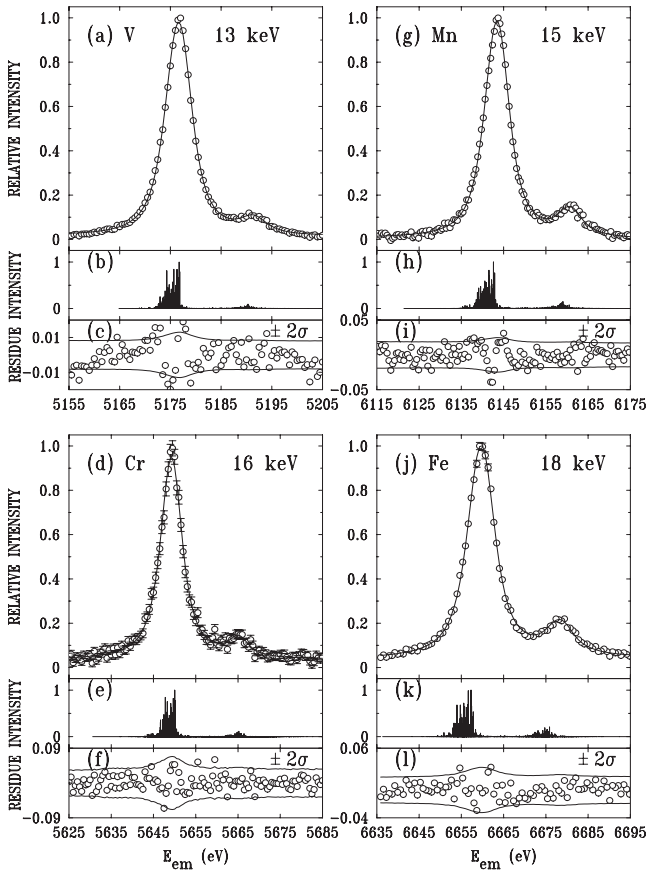

FIG. 1. The $K^h\alpha_{1,2}$ hypersatellite spectra for $Z=23-26$. For each element, the upper panel shows the measured spectrum (circles) and the fit (line) using the *ab initio* RMCDF-calculated stick diagram (middle panel). The fit residuals (circles) and the $\pm 2\sigma$ limits (lines) are shown in the lowest panel. σ is the experimental uncertainty at each data point due to counting statistics. The excitation energy, well above the threshold, is listed for each spectrum.

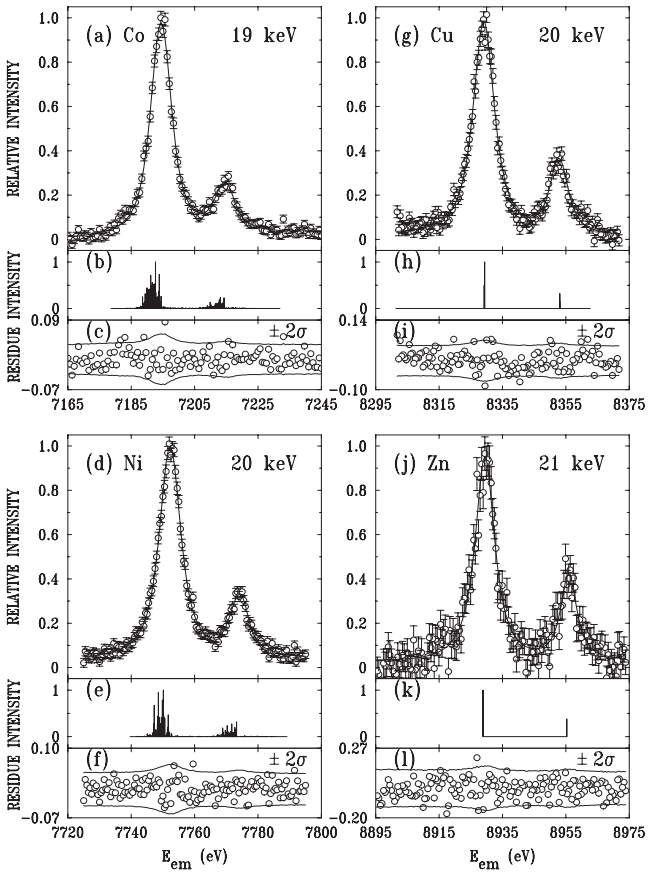

FIG. 2. Same as Fig. 1, for $Z=27-30$.

$\Delta=E(K^h\alpha_2)-E(K\alpha_2)$ of the HS spectrum from the diagram spectrum, and the intensity ratio $R=I(K^h\alpha_1)/I(K^h\alpha_2)$ of the two lines of the $K^h\alpha_{1,2}$ HS doublet.

4. Ab initio fit

Fits of the measured spectra by *ab initio* calculated transition arrays should allow a better understanding of the physics underlying the spectra. In the fits of a RMCDF-calculated spectrum to the measured one each transition line (stick) in the calculated spectrum was represented by a single VF. In order to obtain an unbiased fit by the RMCDF-calculated spectrum the height of the VF was fixed at that of the corresponding stick and a single width, common to all Lorentzians, was employed. A single overall theory-experiment shift (on order of 1–2 eV) between the measured and calculated spectra was also allowed to vary in the fit, along with an overall intensity factor, both common to all lines of the calculated spectrum. In other words, the separation of the lines and the relative intensities *within* each stick diagram spectrum were kept as calculated by GRASP. For further details see Refs. [11,44,45,57].

III. RESULTS AND DISCUSSION

A. Theoretical fit of the measured spectra

The measured HS spectra, following corrections and background subtraction as discussed above, were fitted by the *ab initio* calculated transition array of the $[1s]^{-2}\rightarrow[1s2p]^{-1}$ transition. The results are shown in Figs. 1 and 2, where the calculated stick diagram and fit residuals are also shown for each sample.

The decreasing statistics of the measured spectra with increasing Z, observed as progressively larger point scatter and error bars, reflects the decrease in intensity of the wiggler source with increasing energy when working well above the wiggler's critical energy.

The most outstanding feature of all spectra is the very low intensity of the $K^h\alpha_1$ line in comparison with the stronger $K^h\alpha_2$ line. This is in strong contrast with the diagram $K\alpha_{1,2}$ spectra, where the well-known intensity ratio $I(K\alpha_1)/I(K\alpha_2)\approx 2$ is obtained in our Z range, reflecting the $[2p_{3/2}]/[2p_{1/2}]=2$ subshell population ratio [58]. As mentioned in Sec. I, this is due to the fact that the $[1s]^{-2}(^1S_0)\rightarrow[1s2p]^{-1}(^3P_1)$ transition, which gives rise to the $K^h\alpha_1$ line, is spin-flip dipole forbidden in the *LS* coupling [10,59,60]. The observed intensity is due to a mixing between the triplet $^3P_1$ and singlet $^1P_1$ in the final $[1s2p]^{-1}$ state of the transition. Thus, the various effects, e.g., relativity and Breit interaction, which influence the final state mixing, have an important influence on the relative intensity of the $K^h\alpha_1$ line. With

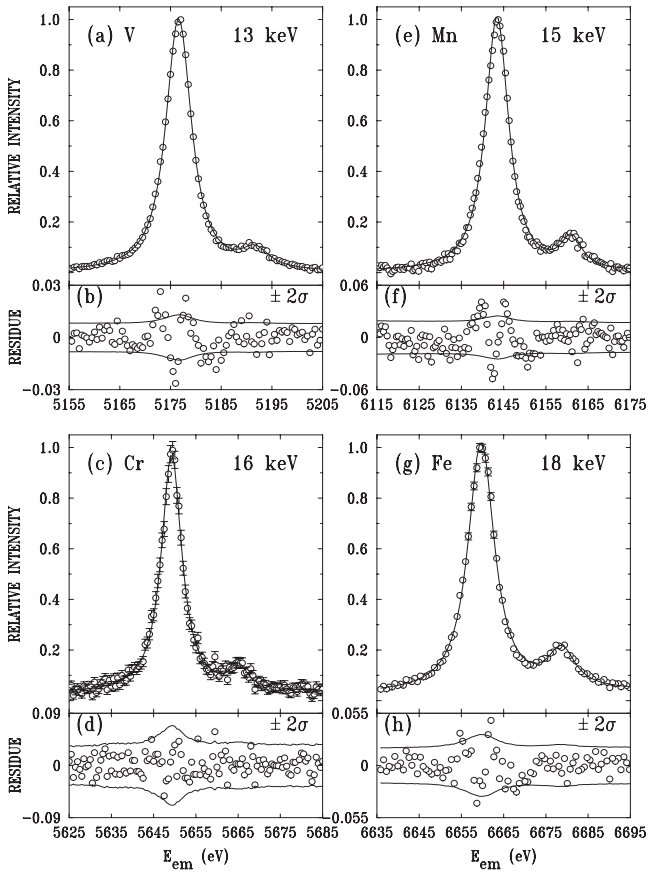

FIG. 3. The $K^h\alpha_{1,2}$ hypersatellite spectra for $Z=23-26$, measured at the same energies as in Figs. 1 and 2. For each element, the upper panel shows the measured spectrum (circles) and its fit (line) by a single Voigt function per line. The fit residuals (circles) and the $\pm 2\sigma$ limits (lines) are shown in the lower panel.

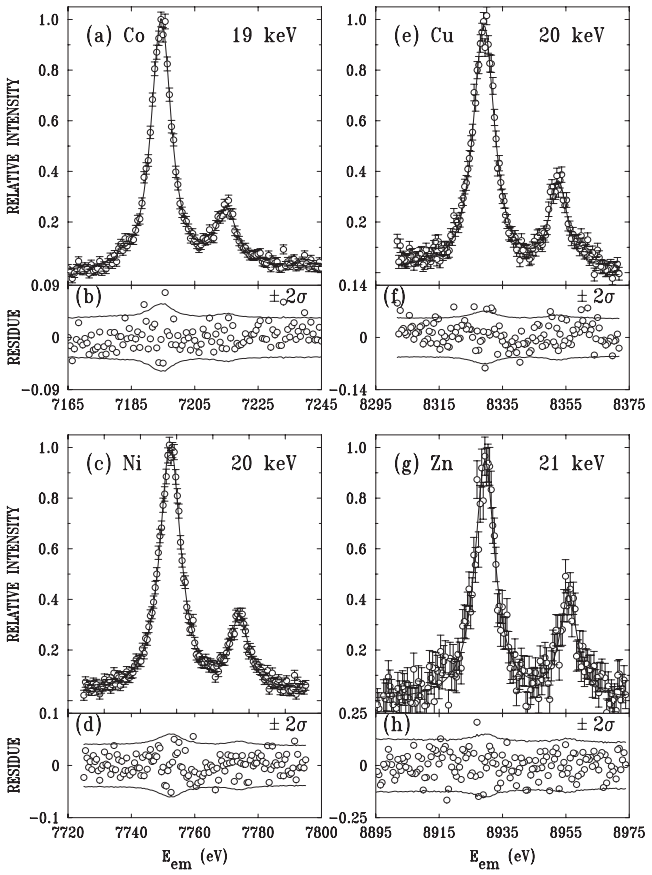

FIG. 4. Same as Fig. 3, for $Z=27-30$.

an increasing Z, as the intermediate coupling moves away from the LS and toward the jj coupling, the $K^h\alpha_1$ line becomes progressively more allowed and its intensity increases. This trend can be clearly observed in Figs. 1 and 2. The number of lines in the calculated stick spectra in the figures, increasing from ~2000 for V to ~28 000 for Cr, then decreasing monotonically from ~7500 for Mn to just 2 for Zn, follows the variation with Z of the occupancy of the open shells in the atoms.

The quality of the fits of the measured spectra by the *ab initio* calculated ones is very good, as shown both by the agreement of the solid line with the measured data and the fact that almost all fit residuals are within the $\pm 2\sigma$ limits of the measured points. Note, in particular, that no systematic deviations are observed in the residuals over extended energy regions in the measured spectral ranges. This indicates that within our experimental accuracy there are no contributions to the spectra from any transitions other than the $[1s]^{-2} \rightarrow [1s2p]^{-1}$, which can be regarded as the diagram transition of a K-hollow atom. In contrast, the diagram spectra of the same nonhollowed neutral atoms include a significant (~30%) intensity contribution from the $[3d]^{-1}$ spectator transition, $[1s3d]^{-1} \rightarrow [2p3d]^{-1}$, in addition to the main contribution from the diagram $[1s]^{-1} \rightarrow [2p]^{-1}$ transition [43,57,61]. Finally, we also note that the good quality of the *ab initio* calculations is reflected in the rather small theory-experiment shifts that were required to bring the calculated spectrum into alignment with the measured one. These were as small as 0.7 eV (for Cr and Zn), with the largest shift being 3 eV (for Ni). This point is further discussed below.

B. Phenomenological fit of the measured spectra

Considering the conclusion above that only a single $[1s]^{-1}$ spectator transition generates the measured $K^h\alpha_{1,2}$ HS spectra, with the two lines of each spectrum originating in the $[1s2p_{1/2}]^{-1}$ and $[1s2p_{3/2}]^{-1}$ final states, and the symmetric shape of the measured lines, a phenomenological fit of each spectrum by a single Voigt function per line was carried out. This fit allows an accurate determination of the characteristics of the lines (position, width, intensity ratio, line splitting, etc.) without restriction to a particular model like the RMCDF used in the calculation discussed above. It also allows separating out conveniently the resolution width of the spectrometer from the lifetime width of the line as the widths of the Gaussian and Lorentzian components of the Voigt function. Finally, this fit allows a convenient comparison with previous measurements and theoretical calculations, which report the values of these same quantities.

The phenomenological fits are shown in Figs. 3 and 4, and the parameter values derived therefrom are listed in Table II. As the residuals show, the fits are good, supporting the conclusion above that the spectra are free from contamination by

TABLE II. Values derived from the measured HS spectra by the phenomenological VF fits for the $K^h\alpha_{1,2}$ peak positions, line splitting δ, Lorentzian components' widths Γ_2 and Γ_1, and integrated intensity ratio R of the two emission lines of each spectrum. All values except R are in eV. See text for further details.

Sample	$K^h\alpha_2$	$K^h\alpha_1$	δ	Γ_2	Γ_1	R
V	5176.6(1)	5191.7(1)	15.1(1)	5.5(1)	6.0(6)	0.08(1)
Cr	5649.2(1)	5665.1(3)	15.9(3)	5.7(1)	5.0(9)	0.08(2)
Mn	6143.4(1)	6160.9(1)	17.5(1)	5.1(1)	5.3(5)	0.13(1)
Fe	6659.7(1)	6678.8(2)	19.1(2)	6.1(2)	6.3(9)	0.16(3)
Co	7194.4(1)	7214.9(2)	20.5(2)	6.7(1)	7.1(6)	0.23(2)
Ni	7752.3(1)	7774.1(1)	21.8(1)	7.5(1)	6.2(4)	0.24(2)
Cu	8329.1(1)	8352.6(2)	23.5(4)	6.9(8)	5.5(8)	0.29(2)
Zn	8929.5(1)	8955.8(3)	26.3(3)	7.5(4)	6.4(7)	0.37(5)

higher-order multivacancy transitions. These contaminations plague HS spectra measurements employing heavy ion or even proton excitation [14,33] as mentioned in Sec. I.

C. Comparison with previous results

The number of previous experimental studies of the $K^h\alpha_{1,2}$ HS spectra with an energy resolution and statistical accuracy sufficient to resolve the two lines of the spectrum and determine their relative intensities is rather small. Such data are progressively more rare as Z increases since the probability of exciting the initial two-hole $[1s]^{-2}$ state and thus the intensity of the HS spectrum decreases rapidly as $\sim Z^{-4}$ [15,50]. Results obtained in our and in previous studies, both measured and calculated, are listed in Table III. Since the more aggressive excitation modes of heavy ion and proton bombardment result in contamination of the HS spectra by higher-order spectral lines [33], only photoexcitation and electron excitation, as well as electron capture, studies were included in Table III. We now briefly discuss each element in more detail.

Vanadium. Two of the three measurements of the $K^h\alpha_2$ line's energy agree, within their much larger experimental uncertainties, with our measured value. The measurement of Oura *et al.* [28] deviates from ours although by only $\lesssim 3\sigma_c$, where σ_c is the combined experimental uncertainty. The calculated values agree with our measured one to $\lesssim 1.2$ eV. The calculated value of Oura *et al.* [28] is higher by 3 eV than our measured value. No previous line splitting value is available since none of the previous experimental studies reported an observation of the $K^h\alpha_1$ line, the intensity of which is only 8% of that of the $K^h\alpha_2$. Our measured line splitting agrees well with the theoretical values. Note that this splitting is twice that of the diagram lines [56], 7.56 eV, indicating the strong nonequal contraction of the $2p_{1/2}$ and $2p_{3/2}$ levels in the absence of the screening of the nucleus provided, in the neutral atom, by the two electrons of the K shell. All measured values of Δ agree to within 4 eV while the calculated ones agree to $\lesssim 1.5$ eV, except the value of Oura *et al.* [28] which deviate by ~ 7 eV. However, their Δ is calculated relative to the unresolved $K\alpha_{1,2}$ which they measured. Considering the 7.56 eV splitting and the 1:2 intensity ratio of the diagram lines, the calculated shift of Oura *et al.* [28] relative to the $K\alpha_2$ line becomes $\Delta = 232.8$ eV, only ~ 1 eV larger than all previously calculated values. Our measured and RMCDF-calculated R values agree very well. The sensitivity of the HS to QED corrections and the Breit interaction is reflected in the fact that the relativistic calculation of Åberg and Suvanen [60], which neglects both QED corrections and the Breit interaction in the mixing calculations, yields a value twice too large, while those in [10], which include them, are significantly closer to the measured values. So do the recent multiconfigurational Dirac-Fock calculations of Costa *et al.* [41], which also include the Breit interaction and the QED effects and which agree closely with the Dirac-Hartree-Slater results of Chen *et al.* [10]. Nevertheless, for V both overestimate R and underestimate δ but agree reasonably with the measured Δ. The close agreement between these two calculations persists for higher Z as well, as does the overestimation trend of R. The agreement of their calculated splitting, δ, with experiment improves, however, significantly for the higher-Z elements within our measurement range, as can be observed clearly in Table III.

It should be noted that Keski-Rahkonen *et al.* [62] also carried out Dirac-Fock calculations similar to those of Åberg and Suvanen [60] for V, Mn, and Fe and obtained identical values (which are, therefore, not listed in Table III). Surprisingly, the simple semiempirical Hartree-Fock calculations of Åberg *et al.* [59], which take into consideration only the intermediate coupling, but no interactions and of course no Breit and QED corrections, yield the best agreement with the measured R among all calculations. However, this good agreement is mostly due to their use of the measured spin-orbit splitting parameter ζ rather than the *ab initio* calculated one. The trends in the calculated R values, discussed here for vanadium, are typical of all the elements measured in this study, as can be observed by inspecting the values listed in Table III.

Chromium. All data, theoretical and experimental, agree with our peak position results except that of Salem *et al.* [36]. The same holds for Δ and, to a somewhat lesser extent, also for the theoretical δ, where only Åberg and Suvanen [60] overestimated the splitting by ~ 1 eV. The only other high-resolution measurement in the literature, by Ahopelto *et al.* [49], agrees well with ours for all parameters listed. Our measured R, which agrees well with Ahopelto's and our RM-

TABLE III. Experimental (Expt.) and theoretical (Theor.) values of the HS spectra for the $K^h\alpha_2$ peak position, the splitting δ, the shift Δ, and the intensity ratio R. All values are in eV units except R.

Sample		Source	$K^h\alpha_2$	δ	Δ	R
V	Expt.	Present	5176.6(1)	15.1(1)	232.0(1)	0.08(1)
		M[a]	5177.0(20)		227.6(25)	
		K[b]	5178.0(20)		231.0(20)	
		O[c]	5178.1(5)		229.0(9)	
	Theor.	Present	5175.1	15.1	230.6	0.077
		CCM[d]		14.4[n]	231.7[o]	0.096[o]
		O[c]	5179.4		237.8	
		AS[e]	5176.9	15.3	231.7	0.153
		A[f]				0.077
		Co[g]		14.51	231.57	0.0989
Cr	Expt.	Present	5649.2(1)	15.9(3)	243.7(1)	0.08(2)
		K[b]	5649.0(20)		243.0(20)	
		Ah[h]	5650.0(20)	16.0(20)	245.0(20)	0.09(9)
		S[i]	5645.0(20)		239.5(20)[q]	
	Theor.	Present	5648.5	15.9	243.0	0.083
		CCM[d]		15.6[n]	243.2[o]	0.125[o]
		AS[e]	5649.2	16.9	243.2	0.179
		A[f]				0.105
		N[s]	5648.4	15.8		0.149
Mn	Expt.	Present	6143.4(1)	17.5(1)	255.8(1)	0.13(1)
		K[b]	6142.0(30)		254.0(30)	
		C[j]	6147.0(300)	19.0(20)	257.0(30)	0.19(5)
	Theor.	Present	6140.9	17.5	253.3	0.121
		CCM[d]		17.0[n]	254.9	0.169
		AS[e]	6143.0	18.3	254.6	0.213
		A[f]				0.133
Fe	Expt.	Present	6659.7(1)	19.1(2)	268.8(10)	0.16(2)
		K[b]	6658.0(20)		267.0(20)	
		Ah[h]	6659.0(20)	20.0(20)	268.0(20)	0.18(6)
		S[i]	6655.0(20)	20.0(30)	264.2(20)[q]	0.22(5)
		B[l]			268.0(20)	
	Theor.	Present	6655.7	18.7	264.4	0.19
		CCM[d]		18.4[n]	266.5[o]	0.194[o]
		AS[e]	6658.2	19.8	266.1	0.23
		A[f]				0.180
		Co[g]		18.42	266.57	0.189
		N[s]	6657.0	18.9		0.217
Co	Expt.	Present	7194.4(1)	20.5(2)	279.1(1)	0.23(2)
		S[i]	7192.0(30)	15.0(30)	276.7(30)[q]	0.24(5)
		VI[k]			274.9(16)[r]	
	Theor.	Present	7191.7	20.5	276.4	0.205
		CCM[d]		19.9[n]	278.3[o]	0.234[o]
		AS[e]	7194.8	21.5	277.7	0.278

TABLE III. (*Continued.*)

Sample		Source	$K^h\alpha_2$	δ	Δ	R
		A[f]				0.213
		Co[g]		20.06	278.00	0.229
Ni	Expt.	Present	7752.3(1)	21.8(1)	291.4(1)	0.24(2)
		Ah[h]	7751.0(20)	24.0(20)	290.0(20)	0.33(8)
		B[l]			292.0(30)	
	Theor.	Present	7749.3	21.8	288.4	0.236
		CCM[d]		21.6[n]	290.1[o]	0.279[o]
		AS[e]	7752.9	23.4	289.4	0.308
		A[f]				0.243
		Co[g]		21.86	289.90	0.277
Cu	Expt.	Present	8329.1(1)	23.5(4)	301.3(1)	0.29(2)
		S[i]	8331.0(30)	21.0(40)	303.2(30)	0.27(7)
		B[l]			303.0(30)	
	Theor.	Present	8329.3	23.7	301.6	0.32
		CCM[d]		23.8[n]	302.0[o]	0.327[o]
		AS[e]	8332.4[p]	24.9[p]	300.9[p]	0.34
		A[f]				0.26
		Co[g]		23.72	301.93	0.325
Zn	Expt.	Present	8929.5(1)	26.3(3)	313.7(1)	0.37(5)
	Theor.	Present	8928.9	26.3	313.1	0.336
		CCM[d]		26.4	314.0	0.358
		Ma[m]	8928.5	26.4		
		AS[e]	8933.5[p]	27.6[p]	312.6[p]	0.403
		A[f]				0.331
		Co[g]		26.44	313.8	0.388
		N[s]	8928.9	26.5		0.393

[a]Murti *et al.*, Ref. [82].
[b]Keski-Rahkonen *et al.*, Ref. [62].
[c]Oura *et al.*, Ref. [28].
[d]Chen *et al.*, Ref. [10].
[e]Åberg and Suvanen, Ref. [60].
[f]Åberg *et al.*, Ref. [59].
[g]Costa *et al.*, Ref. [41].
[h]Ahopelto *et al.*, Ref. [49].
[i]Salem *et al.*, Ref. [36].
[j]Cue *et al.*, Ref. [6].
[k]Vukovic and Ilakovac, Ref. [83].
[l]Briand *et al.*, Ref. [7].
[m]Martins *et al.*, Ref. [84].
[n]Interpolated from CCM (footnote d) with $K\alpha_{1,2}$ energies from Ref. [56].
[o]Polynomial interpolation with Z from CCM (footnote d).
[p]Interpolated with Z from AS (footnote e).
[q]Calculated from S (footnote i) and $K\alpha_{1,2}$ energies from Ref. [56].
[r]Center-of-mass to center-of-mass shift.
[s]Natarajan, Ref. [42].

CDF calculations, shows the same trend as vanadium: a slight overestimation by Chen *et al.* [10], a much larger one by Åberg and Suvanen [60] and by Natarajan [42], and an agreement with the semiempirical Hartree-Fock calculations by Åberg *et al.* [59], as well as our RMCDF calculation.

Manganese. The only other previous measurement, by Cue *et al.* [6], did not resolve the two lines experimentally but rather by fitting the highly overlapping spectrum by two Gaussian on top of a strongly and nonmonotonically varying background, fitted simultaneously by a polynomial. Hence there is a high uncertainty in the peak positions and the other parameter values. Two other low-resolution measurements, not listed in Table III, are the internal conversion measurements by Briand *et al.* [63] and by Nigam and Arora [64]. Neither of them resolved the two lines of the spectrum, and their experimental uncertainties are on the order of 20 and 10 eV in the peak's energy positions and shift, respectively. A somewhat better accuracy of ± 3 eV is cited for the recent measurements of Raju *et al.* [65], for $Z=20-24$, which, however, did not resolve experimentally the two lines of the HS doublets. The agreement of our results with theory is similar to that in Cr and V.

Iron. With two previously reported resolved HS spectrum measurements, iron is the best studied among our samples. The results of Ahopelto *et al.* [49] and Keski-Rahkonen *et al.* [62] and the δ of Salem *et al.* [36] agree with ours within their larger error bars. As in the case of Cr, the results of Salem *et al.* [36] underestimate the peak position and Δ by 4–5 eV. They also list the highest R value, 0.22(5), which, however, still agrees with the other two measured values within the combined experimental uncertainty. The theoretical values show again the same trends as discussed for vanadium except that our calculations are lower by 4 and 4.4 eV than the measured peak position and Δ, respectively, as compared to 1.5 and ~2.4 eV, respectively, of Åberg and Suvanen [60] and a 2.7 eV underestimation of the $K^h\alpha_2$ line energy by Natarajan [42].

Cobalt. The present study and that of Salem *et al.* [36] are the only resolved measurements, with Salem's citing significantly lower values for peak position, δ and Δ, as they do also for Cr and Fe. The R values agree with each other and with the theoretical values, except for that of Åberg and Suvanen [60] which is significantly higher. Our calculated peak position underestimates the measured value by almost 3 eV, while Åberg and Suvanen [60] agreed with our measured value to within 0.4 eV.

Nickel. The present study and that of Ahopelto [49] are the only resolved measurements. All measured peak positions and Δ values agree with each other. Although Ahopelto's δ and R are higher than ours, they still agree within the combined uncertainties. As for Fe and Co, our theoretical peak position and Δ underestimate the measured values by ~3 eV but agree well with the measured Δ and R.

Copper. An overall good agreement is found between Salem's [36] and our measurements and with almost all theoretical calculations, with Åberg-Suvanen [60] values overestimating the measured ones (except Δ) as for some of the previously discussed elements. All calculations overestimate R by ~10%, except Åberg *et al.* [59], which underestimated it by about the same amount. A more complete discussion of the copper results has been published in Ref. [11].

Zinc. We are not aware of any previously published resolved HS measurement for Zn. Verma [66] obtained 8893.3 eV for the peak of the unresolved $K^h\alpha_{1,2}$ HS spectrum. Overall good agreement is obtained with all theoretical calculations except with that of Åberg and Suvanen [60], which overestimated all measured values except Δ.

D. Evolution of the spectra with the excitation energy

As discussed in Sec. II, the experimental methods used here allow us to determine the evolution of the spectra with the excitation energy from threshold to saturation [11]. The evolution of the HS spectrum's intensity is relatively easy to determine by positioning the spectrometer at the $E_{em}(K^h\alpha_2)$ peak and scanning the excitation energy E_{ex}. However, the measurement of a full HS spectrum at a near-threshold energy, in which E_{em} is scanned for a fixed E_{ex}, is a much more demanding task due to the low inherent intensity of the HS, 10^{-4}–10^{-5} of the diagram lines [50,67], even at saturation. Near threshold these intensities are considerably lower.

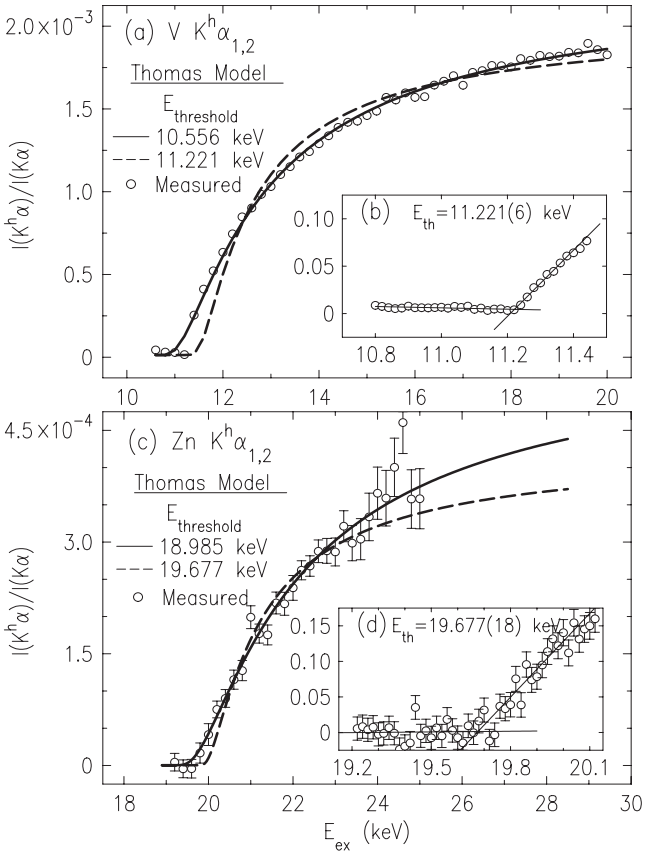

FIG. 5. Measured (circles) and Thomas model fitted (lines) evolution curves from threshold of the $K^h\alpha_{1,2}$ HS intensity normalized by that of the corresponding $K\alpha_{1,2}$ diagram spectrum. The near-threshold region is magnified in the inset, where the y-scale units are fractions of the saturation intensity.

Two typical evolution curves, known also as PFY curves, for V and Zn, are shown in Fig. 5. The continuous and monotonic rise from zero at threshold over an extended excitation-energy range clearly stands out. These are quite unlike the familiar abrupt K edges observed for the thresholds of the diagram $K\alpha_{1,2}$ lines. The finite, and rather large, range over which the intensity reaches a saturation value can be rationalized as follows. The only additional energy scale which exists in the HS transition as compared to the diagram one is the binding energy of the indirectly ionized $1s$ electron creating the $[1s]^{-1}$ spectator of the HS transition. It is therefore plausible to assume that it determines the energy range of the spectral evolution. This argument is supported in general by our measurements on copper, where the $3d$ satellites, the conventional satellites, and the HSs, originating in the $[1s3d]^{-1}$, $[1s2p]^{-1}$, and $[1s]^{-2}$ initial states, respectively, were found to exhibit saturation ranges of 2%, 10%, and 60% of the threshold energy [11,43–45]. A much stronger support for this argument has been presented in our recent publication [50], which demonstrates that upon scaling of the excitation-energy axis by the binding energy of the correlation-ionized $1s$ electron all our measured PFY curves collapse onto a single universal curve, as also does the PFY curve measured for Ag by Kanter *et al.* [17].

The most widely used theoretical treatment of multielectronic excitations accompanying a direct ionization of a

single inner-shell electron is the shake theory. This theory can be used to calculate the probability of shaking up (to unoccupied levels) or off (to the continuum) the second 1s electron upon a direct ionization of the first 1s electron [67,68]. The shake theory predicts an increase in the relative shake-off/shake-up cross section with a decrease in the principal quantum number n. Mukoyama *et al.* [68] predicted a virtually pure *shake-off* process for the HS excitations in our Z range. It has been confirmed both theoretically [67,68] and experimentally [43,69] that the cross section for the shake-off process rises smoothly from zero at the threshold, while that of shake-up exhibits a finite jump at the threshold. Thus, the fact that all our measured PFY curves exhibit an intensity rising smoothly from zero, even on the enlarged scale of the insets of Fig. 5, supports the conclusion that shake-up does not contribute significantly ($<3\%$) to the excitation process of the HS. It must be noted, however, that this does not automatically imply that the HS spectra are excited by a pure shake-off process. In fact, the measurements provide two pieces of evidence that this is not the case.

The first is the saturated intensity of the HS spectrum relative to that of the diagram spectrum. The saturation values of the relative HS intensities for the curves shown in Fig. 5, 1.8×10^{-3} for V and 4.3×10^{-4} Zn, are significantly higher than the values of 5×10^{-5} and 3×10^{-5} predicted theoretically for the corresponding total shake relative cross section [68]. Our measurements of the HS spectra of Cu [11] found a saturation value for the relative cross section which is four times higher than the value calculated for the total relative shake probability. Kanter *et al.* [15,17] similarly found for Mo and Ag a strong underestimation, increasing with Z, by shake theory.

The second piece of evidence against a shake origin for the HS excitation process near threshold is the disagreement of the PFY curve with the Thomas model [47]. This model is based on the shake theory and employs a time-dependent perturbation expansion calculation to predict the excitation-energy dependence of the relative integrated intensity as

$$I(K^h\alpha_{1,2})/I(K\alpha_{1,2}) = I_\infty \exp[-r^2(\Delta E)^2/(15.32\varepsilon)], \quad (1)$$

where I_∞ is the saturation intensity, r is the radius of the shake-off 1s shell in Å, ΔE is the binding energy of the shaken electron, and the excess excitation energy $\varepsilon = E_{ex} - E_{threshold}$ is the difference of the excitation energy E_{ex} and the threshold energy $E_{threshold}$. This theory was found to account well for outer-shell electrons [70] and low-Z atoms [71] but failed for measured PFY curves involving $[2p]^{-1}$ spectators in Co, Fe [46], and Cu [44,45] and $[1s]^{-1}$ spectators in Cu [11]. Figure 5 shows two fits of the Thomas model to the measured PFY curves: in the first (dashed lines), the measured threshold energy was kept fixed and I_∞ and r were allowed to vary, and in the second $E_{threshold}$ was also allowed to vary. As can be observed, when the measured threshold energy is employed, the shape of the measured PFY curve is not reproduced well by the Thomas model, and a too low value of I_∞ is obtained. When the threshold energy is allowed to vary, the agreement of the model with the measured PFY curve improves considerably, but the $E_{threshold}$ value obtained from the fit is ~700 eV lower than the measured value.

TABLE IV. Threshold energies, in keV, for HS excitations.

Sample	Measured	Costa[a]	$Z+1$	$(Z+1)^2$
V	11.221(5)	11.26	11.228	11.225
Cr	12.275(19)	12.31	12.292	12.289
Mn	13.374(31)		13.405	13.404
Fe	14.550(10)	14.60	14.564	14.565
Co	15.753(27)		15.773	15.776
Ni	17.086(62)		17.034	17.038
Cu	18.351(15)	18.38	18.345	18.352
Zn	19.677(36)	19.76	19.721	19.730

[a]Multiconfigurational Dirac-Fock calculations in Ref. [41].

Thus, we conclude that the Thomas model is inadequate for describing the intensity evolution of the HS spectra near threshold. While it is possible that this is due to the failure of one or more of the approximations employed in the Thomas model (e.g., an error function time dependence for the Hamiltonian), it is also plausible that the failure is due to the use of shake theory. Indeed, a recent study of the HS spectrum of Ag by Kanter *et al.* [17] indicates that the PFY curve can be well described by a dominant near-threshold contribution from a knockout (KO or two-step-one, TS1) process [14,51,52], whereby the directly ionized 1s electron knocks out the second 1s electron on its way out. A similar conclusion has been reached in our recent study [50] of the universal scaling behavior of the 3d transition metals' PFY curves. Unfortunately, the available calculations of the cross section's energy dependence by Schneider *et al.* [52] were carried out for He only, and their scaling to the elements studied here may not be reliable. For a more complete discussion of the evolution curves of the elements studied here see Ref. [50].

E. Threshold and $K^h\alpha_2$ energies

The threshold energies obtained from the fine scans in the near-threshold regions, like those shown in the insets of Fig. 5, are listed in Table IV. The $Z+1$ approximation [7,72] estimates the binding energy of the indirectly ionized electron in atom Z as being larger than that of the directly ionized one by a fraction ΔZ of the difference in the binding energies in atoms Z, $E_b^{1s}(Z)$ and $Z+1$, $E_b^{1s}(Z+1)$. Thus, the threshold energy, which is the energy required to generate the initial $[1s]^{-2}$ state, is given by

$$E_{threshold}^{Z+1} = \Delta Z[E_b^{1s}(Z+1) - E_b^{1s}(Z)] + 2E_b^{1s}(Z). \quad (2)$$

For the $[1s]^{-2}$ state $\Delta Z=0.57$ is predicted [7]. As can be observed in the difference plot in Fig. 6(a) the $Z+1$ approximation agrees with all the measured threshold energies to within $\pm 2\sigma$.

A more stringent test for the $Z+1$ approximation is, however, the calculation of the HS lines' energies, which are measured here with an accuracy of 2–3 orders of magnitude higher than that of the threshold. For this we need also the energy of the final state, $[1s2p]^{-1}$, which is calculated similarly to Eq. (2) but with $\Delta Z=1$ for the binding energies of the

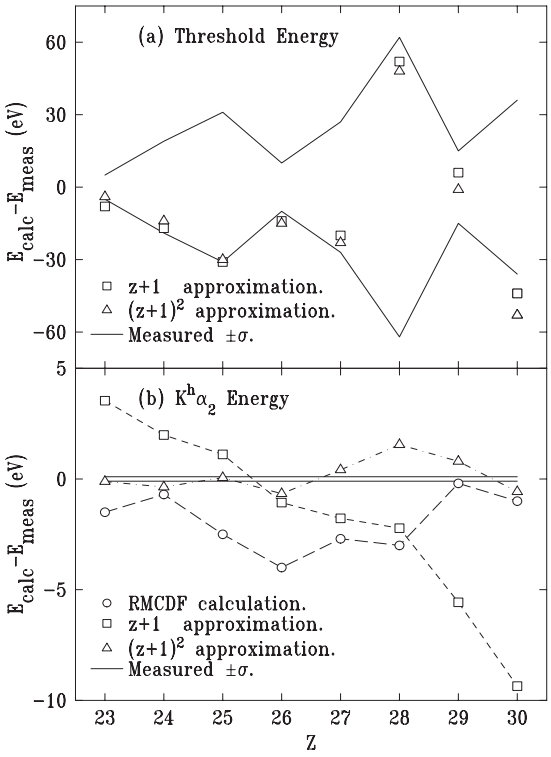

FIG. 6. Deviations of the calculated (a) threshold and (b) $K^h\alpha_2$ energies from the measured values. The $\pm\sigma$ error bars of the measured values in (a) and (b) are shown in solid lines.

$2p$ electron in atoms Z and $Z+1$ [72]. The energy predicted for the $K^h\alpha_2$ peak position is

$$E^{Z+1}_{K^h\alpha_2} = E([1s]^{-2}) - E([1s2p_{1/2}]^{-1}) = 0.57[E^{1s}_b(Z+1) - E^{1s}_b(Z)] + E^{1s}_b(Z) - E^{2p_{1/2}}_b(Z+1), \quad (3)$$

where $E^{2p_{1/2}}_b(Z+1)$ is the binding energy of the $2p_{1/2}$ electron in atom $Z+1$. The deviations of the $Z+1$-estimated peak energies calculated from Eq. (3) from the measured $K^h\alpha_2$ peak positions listed in Table II are shown in Fig. 6(b). Although the maximal deviation, ~10 eV for Zn, is only 0.1% of the peak's energy, it exceeds the experimental uncertainty by 2 orders of magnitude. It is also considerably larger than the *ab initio* calculated RMCDF values which exhibit a maximal deviation of 4 eV. A simple and more accurate method than the $Z+1$ approximation for predicting the HS energies would therefore be useful for further studies and/or line identification in complex spectra. Noting the monotonic trend in the deviations in Fig. 6(b) and regarding the first term in the second line of Eq. (3) as the first term in a truncated power series, we have attempted to approximate the transition energies by the phenomenological expression

$$E^{(Z+1)^2}_{K^h\alpha_2} = E([1s]^{-2}) - E([1s2p_{1/2}]^{-1}) = a[E^{1s}_b(Z+1) - E^{1s}_b(Z)] + b[E^{1s}_b(Z+1) - E^{1s}_b(Z)]^2 + E^{1s}_b(Z) - E^{2p_{1/2}}_b(Z+1) \quad (4)$$

with a and b being adjustable parameters. With this expression, denoted here as the $(Z+1)^2$ approximation, and the values $a=0.508$ and $b=1.03\times10^{-3}$, an improved agreement, with a maximal deviation of 1.5 eV only, has been obtained for the $K^h\alpha_2$ peak position, as can be observed in Fig. 6(b). This is better than the agreement with the *ab initio* RMCDF calculations. As shown in Fig. 6(a), the agreement with the threshold energies, already within the experimental error bars for the $Z+1$ approximation, remains the same for the $(Z+1)^2$ approximation. Finally, we note that the recent *ab initio* multiconfigurational Dirac-Fock threshold energy calculations of Costa *et al.* [41], which include the Breit interaction and QED effects (albeit approximately), reproduce reasonably well (within 2σ and with a slight overestimation) the measured threshold energies.

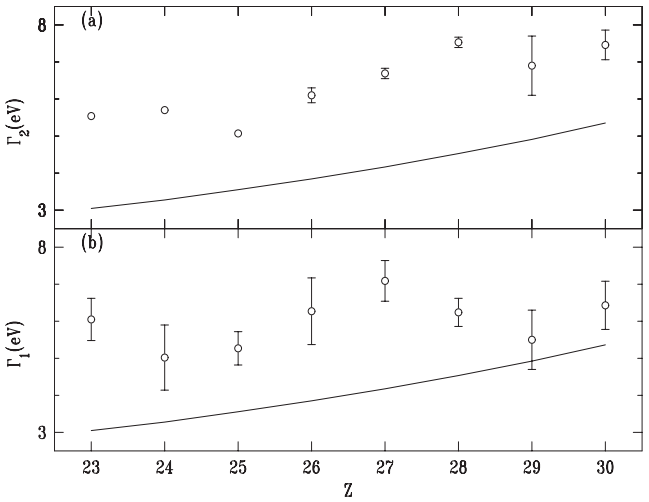

FIG. 7. Lifetime widths Γ_2 and Γ_1 of the (a) $K^h\alpha_2$ and (b) $K^h\alpha_1$ lines, respectively, obtained from the phenomenological fits to the HS spectra (circles). Solid lines are calculated from the model of Mossé *et al.* [35] [Eq. (5)] using level widths from the semiempirical evaluation of Krause and Oliver [73].

F. Linewidths

The widths of measured HS lines are more than twice larger than those of the corresponding diagram lines. This is understandable considering that two level widths are involved in both the initial and the final states, as compared to a single level width for the diagram lines [35]. The phenomenological Voigt function fits, with the Gaussian widths kept fixed at the spectrometer resolutions listed in Table I, yield Lorentzian widths Γ_1 and Γ_2 for the $K^h\alpha_1$ and $K^h\alpha_2$ HS lines, respectively. These can be regarded as the intrinsic lifetime widths of the corresponding transitions. They are listed in Table II.

Mossé *et al.* [35] proposed an empirical model to predict the lifetime widths of HS lines based on the levels participating in the transition $[1s]^{-2}\rightarrow[1s2p]^{-1}$,

$$\Gamma_{1,2} = 3\Gamma_{1s} + \Gamma_{2p_{3/2,1/2}}, \quad (5)$$

where Γ_{1s} and $\Gamma_{2p_{3/2,1/2}}$ are the lifetime widths of the $[1s]^{-1}$ and $[2p_{3/2,1/2}]^{-1}$ hole states, respectively. They found a reasonable agreement between Eq. (5) and their measured width of the Cu $K^h\alpha_2$ line. Figure 7 compares values calculated

from Eq. (5) using level widths from the semiempirical evaluation of Krause and Oliver [73] with our results. Equation (5) systematically underestimates our measured values by 2–3 eV. This implies that the lifetimes of the vacancy states involved in the transitions are shorter than expected theoretically. A similar underestimation of the experimental widths was previously noted by Auerhammer *et al.* [34] for Na and by us [11] for Cu. Using *ab initio* calculated theoretical values for the single-vacancy widths, e.g., from the EADL project [74], yields similar results to those obtained with widths taken from Krause and Oliver [73]. Rzadkiewics *et al.* [75] argued that Eq. (5) is valid for the *jj* coupling limit only and obtained a modified equation for the intermediate coupling regime. However, this expression predicts an even lower $\Gamma_{1,2}$ than Eq. (5) and thus increases the experiment-theory discrepancy as the authors themselves point out. Anagnostopoulus [76] showed that the $[1s]^{-1}$ hole's lifetime width is influenced significantly by the presence of additional vacancies in the same atom. This implies that the lifetime widths to be used in Eq. (5) and its modifications should not be those of the corresponding single vacancies but rather those of the same vacancies in the presence of the relevant additional vacancies. However, Anagnostopoulus's study [76] addresses only the $[1s]^{-1}$ widths in the presence of an additional $[2p]^{-1}$ vacancy. Moreover, it yields a decrease in Γ_{1s} with additional vacancies, which would lead in our case to an increase in the experiment-theory discrepancy. High-resolution measurements of the natural linewidths of atomic levels, like those of Küchler *et al.* [77] and Chantler *et al.* [78], may help to quantify the difference between the measured HS widths and their theoretical estimates more accurately. At present, however, no good physical explanation can be offered for the increased widths and the corresponding faster decay of the double vacancy states relative to those expected from the theoretical considerations.

G. Z-dependent trends

Figure 8 shows the HS spectra measured well above threshold, shifted to the peak position of the $K^h\alpha_2$ line, and normalized to its peak intensity in each spectrum. The figure exhibits the nonlinear increase with an increasing Z in the splitting δ and intensity ratio R of the two lines of the spectra. A similar Z trend is found also for the shift Δ of the lines from the corresponding diagram lines although here the deviation from a linear Z dependence is small.

The importance of the QED corrections for the HS spectra is demonstrated in Fig. 9(a) for Ni. In contrast with the good fit obtained with the RMCDF calculations including these corrections, the same calculations neglecting them yield an ~7 eV upshift in energy (in addition to the ~3 eV theory-experiment shift) relative to the measured spectrum. Moreover, even when downshifted by the large amount of ~7 eV required to make the calculated $K^h\alpha_2$ coincide with the measured one, the QED-less spectrum's splitting is too large to allow a good agreement with the measured spectrum, as shown in Fig. 9(a). This splitting is ~1.5 eV, or 15σ, larger than the measured value. Similar results were obtained for Cu [11].

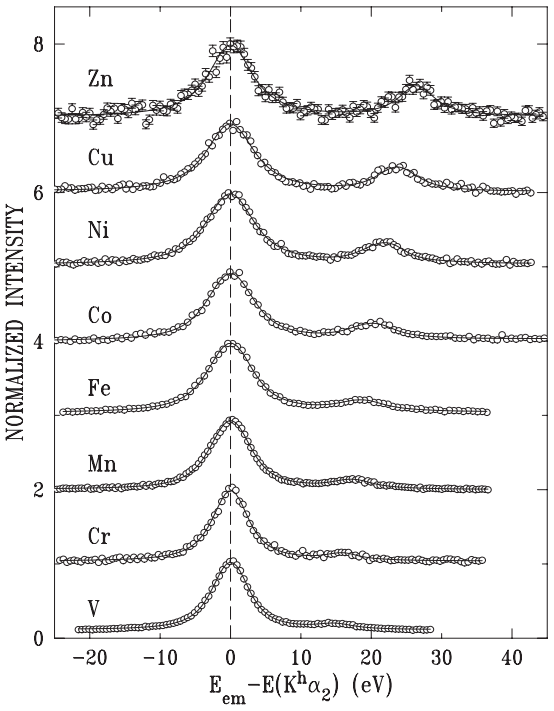

FIG. 8. The measured (open circles) and RMCDF-fitted (lines) $K^h\alpha_{1,2}$ HS spectra for all elements studied. The intensity is normalized to unity at the $K^h\alpha_2$ peak of each spectrum. Spectra are shifted for clarity by unity each.

For Δ, the calculations of Åberg and Suvanen [60], which neglect the QED and Breit interaction in the mixing calculations while still being fully relativistic, agreed with all previous Δ measurements within their rather large error bars, as shown in Fig. 10(a). They showed similar-magnitude deviations from our more accurate measurements as do the Dirac-Hartree-Slater calculations of Chen *et al.* [10], which include the Breit interaction fully. Our RMCDF calculations underestimate the measured shifts slightly more (~1 eV) than those of Chen *et al.* [10] and of Åberg and Suvanen [60]. The reason for that is unclear. However, the effect of the QED and Breit inclusion is clearly reflected in the δ values, shown in Fig. 10(b). While the few previous measurements have error bars too large to distinguish between the three theoretical calculations, Åberg and Suvanen [60] clearly overestimated all of our more accurately measured δ values. The results of Chen *et al.* [10] deviate considerably less than those of Åberg and Suvanen and provide a reasonable agreement with at least the higher-Z elements in the figure. The multiconfigurational Dirac-Fock calculations of Costa *et al.* [41] yield δ and Δ values within a few tenth of an eV from those of Chen *et al.* [10]. The improved wave functions provided by the GRASP package used in our calculations provide a better agreement with our measured δ values. For example, the deviations of the calculated δ from the measured values are 3σ, 1σ, and 0σ for Cr and 15σ, 3σ, and 1σ for Ni for Åberg, Chen, and us, respectively.

An even more pronounced distinction between the three calculations emerges for R, shown in Fig. 10(c). Here the exclusion of QED and Breit interaction raises the result of Åberg and Suvanen [60] well over the measured values by as

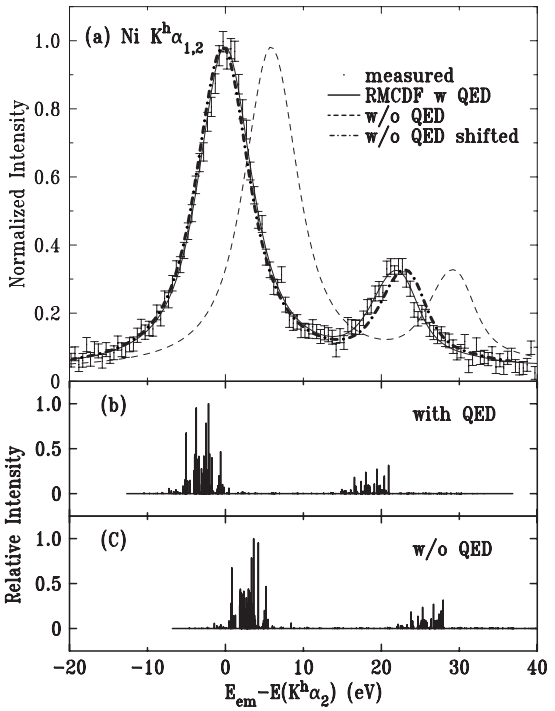

FIG. 9. (a) Comparison of the measured spectrum (symbols) with the RMCDF-calculated spectra with (solid line) and without (dashed line) QED corrections for the Ni $K^h\alpha_{1,2}$ HS spectrum. The bold dashed-dotted line is the same as the light dashed line, but downshifted to make the $K^h\alpha_2$ peak of the calculated and measured spectra coincide. [(b) and (c)] The stick diagrams of Ni $K^h\alpha_{1,2}$, calculated *ab initio* with and without QED corrections.

much as a factor of 2 for V, Cr, and Mn. Part of this could also be attributed to their neglect of the difference in energy and in the matrix elements of the two HS lines [10]. The improved Dirac-Fock wave functions, used by us, as compared to the Dirac-Hartree-Slater ones of Chen *et al.* [10], yield a significant improvement in the agreement of our results with experiment as compared with those of Chen *et al.* [10]. Since R depends sensitively on the intermediacy of the coupling between the LS and jj limits, the good agreement between our calculations and measurements indicates that the intermediacy is taken into account properly by the GRASP package even in the average-level calculation mode and in spite of the large number of transitions occurring in a fully J-split calculation (from a few to a few ten thousands).

The observations above concerning the agreement of theory with experiment are rather general and preliminary in nature. They do not explore in detail the specific contributions of individual effects, such as relativity, coupling, electron interactions, QED, etc., to the excitation and deexcitation processes of the HS spectra. Moreover, no attempt was made to identify the importance of the various individual QED effects such as vacuum polarization, self-energy, and higher-order corrections [79] to the various observables. However, the high-resolution, high-accuracy HS spectra presented here, extending over the Z range where the coupling varies from an almost pure LS to a distinctly intermediate scheme, should stimulate and provide a stringent test for theoretical studies exploring in detail the various contributions and their relative importance.

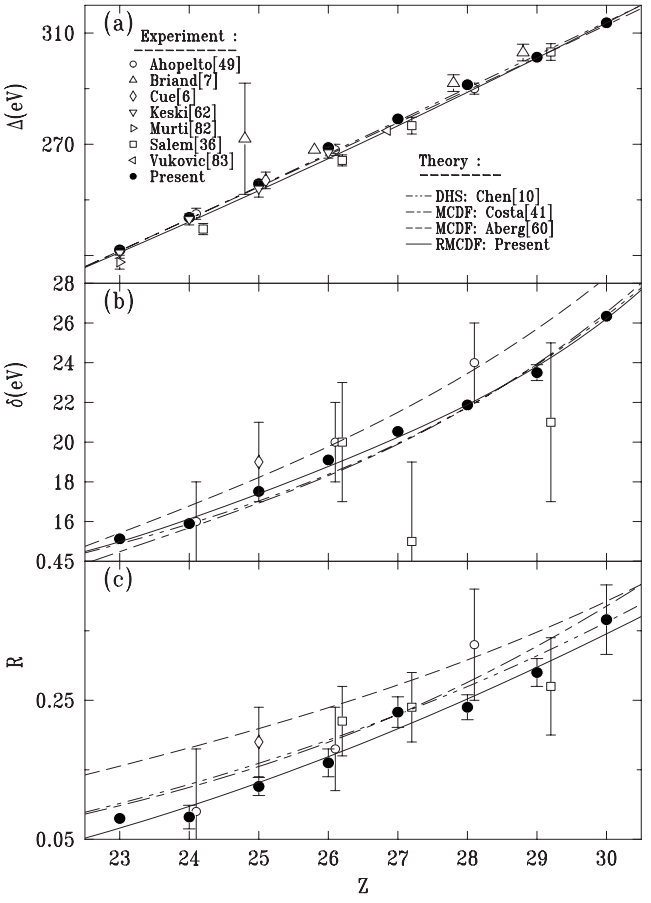

FIG. 10. $K^h\alpha_{1,2}$ HS spectra characteristics. (a) HS-diagram energy shift $\Delta=E(K^h\alpha_2)-E(K\alpha_2)$. (b) Line splitting $\delta=E(K^h\alpha_1)-E(K^h\alpha_2)$. (c) Integrated intensity ratio of the two HS lines of each spectrum $R=I(K^h\alpha_1)/I(K^h\alpha_2)$. The numbers in square brackets indicate the corresponding references.

IV. SUMMARY AND CONCLUSIONS

We present here a systematic high-resolution study of the $K^h\alpha_{1,2}$ HS spectra of the $3d$ transition metals $Z=23-30$. The spectra were analyzed for their phenomenological characteristics, i.e., line splitting δ, shift from the diagram lines Δ, linewidths, and line intensity ratio R. Comparison with *ab initio* calculations indicates that while relativity, as reflected in Δ is mostly accounted for well by relativistic calculations, the QED and Breit contributions, as reflected in δ and R, may need improved calculations. The intermediacy of the coupling of angular momenta, tested sensitively by the agreement with the measured R, is also accounted for well in our RMCDF calculations, while the best previous calculations overestimate the measured R for most elements studied here.

The threshold energies for photoexcitation of the HS spectra and the evolution of their intensities from threshold as a function of the excitation energy were determined. The latter shows an unusually large energy range from threshold to saturation, corresponding roughly to the binding energy of the indirectly ionized $1s$ electron. The measured evolution curve does not agree with the Thomas model for electron shake-off, expected to hold for the near-threshold adiabatic

region. This indicates the dominance of a nonshake mechanism near threshold. The most likely candidate for this mechanism is the knockout of the indirectly ionized electron by the directly ionized one, as shown in more detail in our recent study [50]. The threshold energies are reasonably well obtained from the $Z+1$ approximation. However, this approximation deviates significantly from the more accurately measured $K^h\alpha_2$ energies. A new approximation, denoted as the $(Z+1)^2$ approximation, is suggested. It improves significantly the agreement with the measured values. The linewidths also deviate from the expected behavior, indicating systematically shorter lifetimes for the hole states in a two-hole hollow atom than their counterparts in a single-hole atom. The reasons for this faster decay of hole states are not understood.

The present measurements were carried out on solid targets. Binding effects on x-ray spectra can appear as energy shifts or as intensity changes in emission lines. However, in diagram lines they have a measurable effect only on transitions involving valence electrons [80,81]. In our Z range the effects on $K\alpha$ lines are negligible [80]. Small solid state binding effects on order of $\sim$1 eV shifts and intensity changes of a few percent were found in the outer lines of the $K\beta$ band, which involve valence electrons [80,81]. Since the transitions generating the $K^h\alpha$ HS spectra in our Z range do not involve valence electrons, solid state binding effects are expected to be negligible. This conclusion is further supported by the agreement in Table III of the measured HS line energies, measured on solid targets, with the theoretical values (within their spread), all of which were calculated for single isolated atoms for all elements studied here.

Alongside the several important findings, such as an extended saturation range, and shorter hole lifetimes, a major contribution of this study is the provision of a systematic set of high-accuracy and high-resolution HS measurements over a range of scientifically interesting Z values. This set could be used to test future theoretical models of atomic structure and theories of multielectronic excitations and de-excitations of atoms. Issues that are still not fully understood for lack of experimental data would benefit from the data presented here. These include the evolution of the intensity from threshold to saturation (and the physics underlying this behavior) and the details of the evolution of the coupling of angular momenta across the Periodic Table, as reflected in the Z dependence of R. Since our companion paper [53] extends the present HS measurements to considerably larger values, we will discuss the variation of the coupling scheme across the Periodic Table as reflected in our $R(Z)$ measurements together for the whole Z range of the two papers in the accompanying paper [53].

ACKNOWLEDGMENTS

We gratefully acknowledge support by The Israel Science Foundation, Jerusalem (M.D.) and the Academy of Finland (K.H.) (Contracts No. 201291 and No. 205967), beam time at X25 (NSLS) and at ID16 (ESRF), and expert experimental support and advice by Z. Yin and L. E. Berman (NSLS). BNL is supported by the U.S. DOE under Contract No. DE-AC02-76CH00016.

[1] M. Siegbahn and W. Stenström, Phys. Z. **17**, 318 (1916); M. J. Druyvesteyn, Z. Phys. **43**, 707 (1927); E. Ramberg, Phys. Rev. **45**, 389 (1934); F. Bloch, *ibid.* **48**, 187 (1935); R. D. Richtmyer, *ibid.* **49**, 1 (1936).

[2] B. Crasemann, J. Phys. (Paris), Colloq. **48**, C9-389 (1987); V. Schmidt, Rep. Prog. Phys. **55**, 1483 (1992).

[3] J. W. Cooper, Phys. Rev. A **38**, 3417 (1988); H. P. Saha, *ibid.* **42**, 6507 (1990).

[4] B. Crasemann, in *Atomic Inner-Shell Physics*, edited by B. Crasemann, (Plenum, New York, 1986); Can. J. Phys. **76**, 251 (1998); B. Crasemann, M. H. Chen, and H. Mark, J. Opt. Soc. Am. B **1**, 224 (1984).

[5] J. Stöhr, R. Jaeger, and J. J. Rehr, Phys. Rev. Lett. **51**, 821 (1983).

[6] N. Cue, W. Scholz, and A. Li-Scholz, Phys. Lett. **63A**, 54 (1977).

[7] J. P. Briand, A. Touati, M. Frilley, P. Chevallier, A. Johnson, J. P. Rozet, M. Tavernier, S. Shafroth, and M. O. Krause, J. Phys. B **9**, 1055 (1976).

[8] T. Åberg, K. A. Jamison, and P. Richard, Phys. Rev. Lett. **37**, 63 (1976).

[9] J. P. Desclaux, Ch. Briançon, J. P. Thibaud, and R. J. Walen, Phys. Rev. Lett. **32**, 447 (1974).

[10] M. H. Chen, B. Crasemann, and H. Mark, Phys. Rev. A **25**, 391 (1982).

[11] R. Diamant, S. Huotari, K. Hämäläinen, C. C. Kao, and M. Deutsch, Phys. Rev. Lett. **84**, 3278 (2000); Phys. Rev. A **62**, 052519 (2000).

[12] H. Winter and F. Aumayr, J. Phys. B **32**, R39 (1999); H. L. Zhou, S. T. Manson, L. Vo Ky, P. Faucher, F. Bely-Dubau, A. Hibbert, S. Diehl, D. Cubaynes, J. M. Bizau, L. Journel, and F. W. Wuilleumier, Phys. Rev. A **59**, 462 (1999); H. Khemliche, T. Schlathölter, R. Hoekstra, R. Morgenstern, and S. Schippers, Phys. Rev. Lett. **81**, 1219 (1998); Y. Azuma, S. Hasegawa, F. Koike, G. Kutluk, T. Nagata, E. Shigemasa, A. Yagishita, and I. A. Sellin, *ibid.* **74**, 3768 (1995).

[13] J. P. Briand, L. de Billy, P. Charles, S. Essabaa, P. Briand, R. Geller, J. P. Desclaux, S. Bliman, and C. Ristori, Phys. Rev. Lett. **65**, 159 (1990).

[14] J. A. Tanis, J.-Y. Chesnel, F. Frémont, D. Hennecart, X. Husson, A. Cassimi, J. P. Grandin, B. Skogvall, B. Sulik, J.-H. Bremer, and N. Stolterfoht, Phys. Rev. Lett. **83**, 1131 (1999).

[15] E. P. Kanter, R. W. Dunford, B. Krässig, and S. H. Southworth, Phys. Rev. Lett. **83**, 508 (1999); R. W. Dunford, E. P. Kanter, B. Krässig, S. H. Southworth, and L. Young, Radiat. Phys. Chem. **70**, 149 (2004).

[16] E. P. Kanter, R. W. Dunford, B. Krässig, S. H. Southworth, and L. Young, Radiat. Phys. Chem. **75**, 2174 (2006).

[17] E. P. Kanter, I. Ahmad, R. W. Dunford, D. S. Gemmell, B. Krässig, S. H. Southworth, and L. Young, Phys. Rev. A **73**,

022708 (2006).
[18] S. Martin, R. Bredy, J. Bernard, J. Desesquelles, and L. Chen, Phys. Rev. Lett. **89**, 183401 (2002).
[19] K. Moribayashi, T. Kagawa, and D. E. Kim, J. Phys. B **37**, 4119 (2004).
[20] K. Moribayashi, A. Sasaki, and T. Tajima, Phys. Rev. A **58**, 2007 (1998).
[21] K. Moribayashi A. Sasaki, Y. Ueshima, and T. Tajima, Inst. Phys. Conf. Ser. **159**, 321 (1999); K. Moribayashi, A. Sasaki, and T. Tajima, Phys. Rev. A **59**, 2732 (1999); I. Hughes, Phys. World **8**, 43 (1995).
[22] M. S. Pindzola, F. Robicheaux, and J. Colgan, Phys. Rev. A **72**, 022709 (2005); K. Boyer, A. B. Borisov, X. Song, P. Zhang, J. C. McCorkindale, S. F. Khan, Y. Dai, P. C. Kepple, J. Davis, and C. K. Rhodes, J. Phys. B **38**, 3055 (2005); N. Vaeck and N. J. Kylstra, Phys. Rev. A **65**, 062502 (2002), and references therein.
[23] J.-P. Briand, S. Thuriez, G. Giardino, G. Borsoni, M. Froment, M. Eddrief, and C. Sébenne, Phys. Rev. Lett. **77**, 1452 (1996).
[24] L. M. Kiernan, E. T. Kennedy, J. P. Mosnier, J. T. Costello, and B. F. Sonntag, Phys. Rev. Lett. **72**, 2359 (1994).
[25] Y. Azuma, F. Koike, J. W. Cooper, T. Nagata, G. Kutluk, E. Shigemasa, R. Wehlitz, and I. A. Sellin, Phys. Rev. Lett. **79**, 2419 (1997); R. Wehlitz, M. M. Martinez, J. B. Bluett, D. Lukic, and S. B. Whitfield, Phys. Rev. A **69**, 062709 (2004); E. T. Kennedy, Phys. Scr., T **T95**, 32 (2001).
[26] S. Huotari, K. Hämäläinen, R. Diamant, R. Sharon, C. C. Kao, and M. Deutsch, J. Electron Spectrosc. Relat. Phenom. **137-140**, 293 (2004).
[27] R. Diamant, S. Huotari, K. Hämäläinen, R. Sharon, C. C. Kao, and M. Deutsch, Phys. Rev. Lett. **91**, 193001 (2003).
[28] M. Oura, H. Yamaoka, K. Kawatsura, K. Takahiro, N. Takeshima, Y. Zou, R. Hutton, S. Ito, Y. Awaya, M. Terasawa, T. Sekioka, and T. Mukoyama, J. Phys. B **35**, 3847 (2002).
[29] J. P. Briand, P. Chevallier, A. Touati, and J. P. Rozet, Phys. Rev. Lett. **27**, 777 (1971).
[30] D. L. Wark, R. Bartlett, T. J. Bowles, R. G. H. Robertson, D. S. Sivia, W. Trela, J. F. Wilkerson, G. S. Brown, B. Crasemann, S. L. Sorensen, S. J. Schaphorst, D. A. Knapp, J. Henderson, J. Tulkki, and T. Äberg, Phys. Rev. Lett. **67**, 2291 (1991).
[31] A. Migdal, J. Phys. (USSR) **4**, 449 (1941); E. L. Feinberg, *ibid.* **4**, 423 (1941).
[32] W. Wölfi, Ch. Stoller, G. Bonani, M. Suter, and M. Stöckli, Phys. Rev. Lett. **35**, 656 (1975).
[33] B. Boschung, J.-Cl. Dousse, B. Galley, Ch. Herren, J. Hoszowska, J. Kern, Ch. Rhême, Z. Halabuka, T. Ludziejewski, P. Rymuza, Z. Sujkowski, and M. Polasik, Phys. Rev. A **51**, 3650 (1995).
[34] J. Auerhammer, H. Genz, G. Kilgus, A. Kumar, and A. Richter, Phys. Rev. A **35**, 4505 (1987).
[35] J. P. Mossé, P. Chevallier, and J. P. Briand, Z. Phys. A **322**, 207 (1985).
[36] S. I. Salem, A. Kumar, and B. L. Scott, Phys. Rev. A **29**, 2634 (1984); S. I. Salem, A. Kumar, B. L. Scott, and R. D. Ayers, Phys. Rev. Lett. **49**, 1240 (1982).
[37] K. Hämäläinen, D. P. Siddons, J. B. Hastings, and L. E. Berman, Phys. Rev. Lett. **67**, 2850 (1991); C. C. Kao, W. A. Caliebe, J. B. Hastings, K. Hämäläinen, and M. Krisch, Rev. Sci. Instrum. **67**, 3363 (1996); K. Hämäläinen, M. Krisch, C. C. Kao, W. A. Caliebe and J. B. Hastings, *ibid.* **66**, 1525 (1995).
[38] C. C. Kao, K. Hämäläinen, M. Krisch, P. D. Siddons, T. Oversluizen, and J. B. Hastings, Rev. Sci. Instrum. **66**, 1699 (1995); W. Schülke, *Electron Dynamics by Inelastic X-Ray Scattering* (Oxford University Press, New York, 2007).
[39] F. A. Parpia, C. F. Fischer, and I. P. Grant, Comput. Phys. Commun. **94**, 249 (1996); S. Fritsche, J. Electron Spectrosc. Relat. Phenom. **114**, 1155 (2001); T. Utsumi, T. Yabe, J. Koga, T. Aoki, and M. Sekine, Comput. Phys. Commun. **157**, 121 (2004).
[40] K. G. Dyall, I. P. Grant, C. T. Johnson, F. A. Parpia, and E. P. Plummer, Comput. Phys. Commun. **55**, 425 (1989).
[41] A. M. Costa, M. C. Martins, J. P. Santos, P. Indelicato, and F. Parente, J. Phys. B **40**, 57 (2007).
[42] L. Natarajan, Phys. Rev. A **78**, 052505 (2008).
[43] S. Galambosi, H. Sutinen, A. Mattila, K. Hämäläinen, R. Sharon, C. C. Kao, and M. Deutsch, Phys. Rev. A **67**, 022510 (2003).
[44] M. Deutsch, O. Gang, K. Hämäläinen, and C. C. Kao, Phys. Rev. Lett. **76**, 2424 (1996).
[45] M. Fritsch, C. C. Kao, K. Hämäläinen, O. Gang, E. Förster, and M. Deutsch, Phys. Rev. A **57**, 1686 (1998).
[46] R. Diamant, R. Sharon, W. A. Caliebe, C. C. Kao, and M. Deutsch, J. Phys. B **39**, 651 (2006).
[47] T. D. Thomas, Phys. Rev. Lett. **52**, 417 (1984); T. D. Thomas, J. Electron Spectrosc. Relat. Phenom. **40**, 259 (1986); E. Vatai, Phys. Rev. A **38**, 3777 (1988).
[48] M. H. Chen, Phys. Rev. A **44**, 239 (1991).
[49] J. Ahopelto, E. Rentavuori, and O. Keski-Rahkonen, Phys. Scr. **20**, 71 (1979).
[50] S. Huotari, K. Hämäläinen, R. Diamant, R. Sharon, C. C. Kao, and M. Deutsch, Phys. Rev. Lett. **101**, 043001 (2008).
[51] J. A. R. Samson, Phys. Rev. Lett. **65**, 2861 (1990).
[52] T. Schneider, P. L. Chocian, and J. M. Rost, Phys. Rev. Lett. **89**, 073002 (2002); T. Schneider and J. M. Rost, Phys. Rev. A **67**, 062704 (2003).
[53] R. Diamant, S. Huotari, K. Hämäläinen, R. Sharon, C. C. Kao, V. Honkimäki, T. Buslaps, M. Deutsch, the following paper, Phys. Rev. A **79**, 062512 (2009).
[54] *X-Ray Data Booklet*, edited by A. C. Thompson *et al.* (Lawrence Berkeley National Laboratory, Berkeley, CA, 2001), Rev. 2.
[55] R. D. Deslattes, E. G. Kessler, Jr., P. Indelicato, L. deBilly, E. Lindroth, and J. Anton, Rev. Mod. Phys. **75**, 35 (2003).
[56] J. A. Bearden, Rev. Mod. Phys. **39**, 78 (1967).
[57] M. Deutsch, G. Hölzer, J. Härtwig, J. Wolf, M. Fritsch, and E. Förster, Phys. Rev. A **51**, 283 (1995).
[58] J. H. Scofield, Phys. Rev. A **9**, 1041 (1974); At. Data Nucl. Data Tables **14**, 121 (1974); S. I. Salem, S. L. Panossian, and R. A. Krause, *ibid.* **14**, 91 (1974).
[59] T. Åberg, J. P. Briand, P. Chevallier, A. Chetioui, J. P. Rozet, M. Tavernier, and A. Touati, J. Phys. B **9**, 2815 (1976).
[60] T. Åberg and M. Suvanen, in *Advances in X-Rays Spectroscopy*, edited by C. Bonnelle and C. Mande (Pergamon, New York, 1982).
[61] G. Hölzer, M. Fritsch, M. Deutsch, J. Härtwig, and E. Förster, Phys. Rev. A **56**, 4554 (1997).
[62] O. Keski-Rahkonen, J. Saijonmaa, M. Suvanen, and A. Servomaa, Phys. Scr. **16**, 105 (1977).

[63] J. P. Briand, P. Chevallier, A. Johnson, J. P. Rozet, M. Tavernier, and A. Touati, Phys. Lett. **49A**, 51 (1974).
[64] A. N. Nigam and S. Arora, Indian J. Pure Appl. Phys. **25**, 337 (1987).
[65] S. S. Raju, B. Seetharami Reddy, M. V. R. Murti, and L. Mombasawala, X-Ray Spectrom. **36**, 35 (2007).
[66] H. R. Verma, J. Phys. B **33**, 3407 (2000).
[67] T. Mukoyama and Y. Ito, Nucl. Instrum. Methods Phys. Res. B **87**, 26 (1994), and references therein.
[68] T. Mukoyama and K. Taniguchi, Bull. Inst. Chem. Res., Kyoto Univ. **70**, 1 (1992); T. Mukoyama, Y. Ito, and K. Taniguchi, X-Ray Spectrom. **28**, 491 (1999); T. Mukoyama, *ibid.* **34**, 64 (2005).
[69] G. B. Armen, T. Åberg, K. R. Karim, J. C. Levin, B. Crasemann, G. S. Brown, M. H. Chen, and G. E. Ice, Phys. Rev. Lett. **54**, 182 (1985).
[70] C. Sternemann, A. Kaprolat, M. H. Krisch, and W. Schulke, Phys. Rev. A **61**, 020501(R) (2000).
[71] F. Heiser, S. B. Whitefield, J. Viefhaus, U. Becker, P. A. Heimann, and D. A. Shirley, J. Phys. B **27**, 19 (1994).
[72] M. Deutsch, Phys. Rev. A **39**, 3956 (1989), and references therein.
[73] M. O. Krause and J. H. Oliver, J. Phys. Chem. Ref. Data **8**, 329 (1979).
[74] S. T. Perkins, D. E. Cullen, M. H. Chen, J. H. Hubbell, J. Rathkopf, and J. Scofield, "Tables and Graphs of Atomic Subshell and Relaxation Data Derived from the LLNL Evaluated Atomic Data Library (EADL)," Report No. UCRL-50400, Vol. 30, 1991 (unpublished).
[75] J. Rzadkiewicz *et al.*, Nucl. Instrum. Methods Phys. Res. B **235**, 110 (2005).
[76] D. F. Anagnostopoulos, J. Phys. B **28**, 47 (1995).
[77] D. Küchler, U. Lehnert, and G. Zschornack, X-Ray Spectrom. **27**, 177 (1998).
[78] C. T. Chantler, M. N. Kinnane, C. H. Su, and J. A. Kimpton, Phys. Rev. A **73**, 012508 (2006).
[79] P. Pyykkö and L. B. Zhao, J. Phys. B **36**, 1469 (2003).
[80] S. Fazinic, M. Jaksic, L. Mandic, and J. Dobrinic, Phys. Rev. A **74**, 062501 (2006).
[81] U. Bergmann, C. R. Horne, T. J. Collins, J. M. Workman, and S. P. Cramer, Chem. Phys. Lett. **302**, 119 (1999); S. Raj, B. B. Dhal, H. C. Padhi, and M. Polasik, Phys. Rev. B **58**, 9025 (1998); Y. Kalayci, A. Aydinuraz, B. Tugluoglu, and R. H. Mutlu, Nucl. Instrum. Methods Phys. Res. B **255**, 438 (2007).
[82] M. V. R. Murti, K. S. Rao, V. Radhakrishna Murti, V. Gopalakrishna, M. L. N. Raju, and K. Parthasaradi, Indian J. Phys. A **62A**, 90 (1988).
[83] B. Vuković and K. Ilakovac, Nucl. Instrum. Methods Phys. Res. B **174**, 401 (2001).
[84] M. C. Martins, A. M. Costa, J. P. Santos, F. Parente, and P. Indelicato, J. Phys. B **37**, 3785 (2004).